Structural Adaptations in the Rat Tibia Bone Induced by Pregnancy and Lactation Confer Protective Effects against Future Estrogen Deficiency

Chantal M. J. de Bakker[1], Yihan Li[1], Hongbo Zhao[1,2], Laurel Leavitt[1], Wei-Ju Tseng[1], Tiao Lin[1,3], Wei Tong[1,4], Ling Qin[1], and X. Sherry Liu[1*]

[1] McKay Orthopaedic Research Laboratory, Department of Orthopaedic Surgery, Perelman School of Medicine, University of Pennsylvania, Philadelphia, PA, United States

[2] Key Laboratory of Biorheological Science and Technology, Ministry of Education and Bioengineering College, Chongqing University, Chongqing, China

[3] Department of Musculoskeletal Oncology, The First Affiliated Hospital of Sun Yat-sen University, Guangzhou, China.

[4] Department of Orthopaedics, Union Hospital, Tongji Medical College, Huazhong University of Science and Technology, Wuhan, Hubei, China

*To whom correspondence should be addressed
X. Sherry Liu
McKay Orthopaedic Research Laboratory
Department of Orthopaedic Surgery
University of Pennsylvania
G11A Stemmler Hall, 36th Street and Hamilton Walk
Philadelphia, PA 19104, USA
Email: xiaoweil@pennmedicine.upenn.edu
Phone: 1-215-746-4668

Conflict of Interest:
The authors declare that they have no conflict of interest.

Number of words in abstract:	292
Number of words in manuscript:	6212
Number of tables:	0
Number of black/white figures:	2
Number of color figures:	4

Abstract:

The female skeleton undergoes substantial structural changes during the course of reproduction. Although bone mineral density recovers post-weaning, reproduction may induce permanent alterations in maternal bone microarchitecture. However, epidemiological studies suggest that a history of pregnancy and/or lactation does not increase the risk of postmenopausal osteoporosis or fracture and may even have a protective effect. Our study aimed to explain this paradox by using a rat model, combined with *in vivo* micro-computed tomography (μCT) imaging and bone histomorphometry, to track the changes in bone structure and cellular activities in response to estrogen deficiency following ovariectomy (OVX) surgery in rats with and without a reproductive history. Our results demonstrated that a history of reproduction results in an altered skeletal response to estrogen-deficiency-induced bone loss later in life. Prior to OVX, rats with a reproductive history had lower trabecular bone mass, altered trabecular microarchitecture, and more robust cortical structure at the proximal tibia when compared to virgins. After OVX, these rats underwent a lower rate of trabecular bone loss than virgins, with minimal structural deterioration. As a result, by 12 weeks post-OVX, rats with a reproductive history had similar trabecular bone mass, elevated trabecular thickness and increased robustness of cortical bone when compared to virgins, resulting in greater bone stiffness. Further evaluation suggested that reproductive-history-induced differences in post-OVX trabecular bone loss were likely due to differences in baseline trabecular microarchitecture, particularly trabecular thickness. Rats with a reproductive history had a larger population of thick trabeculae, which may be protective against post-OVX trabecular connectivity deterioration and bone loss. Taken together, these findings indicate that reproduction-associated changes in bone microarchitecture appear to reduce the rate of bone loss induced by estrogen deficiency later in life, and thereby exert a long term protective effect on bone strength.

1. Introduction:

Osteoporosis, a disease of low bone mass and microarchitectural deterioration, affects 35% of postmenopausal women in the United States [1]. Although postmenopausal osteoporosis is largely a result of elevations in the rate of bone remodeling induced by low estrogen levels, the peak bone mass that is achieved prior to menopause also plays an important role in subsequent osteoporosis risk. In fact, the variance in the bone structure attained early in life has been shown to be up to 10 times greater than the variance in the rate of postmenopausal bone loss [2,3]. In addition to bone growth during development, many factors, including nutrition, physical activity, and medication history, affect the peak bone structure and mass that is attained in young adulthood, and therefore may impact the long-term risk of developing postmenopausal osteoporosis.

In addition, the female skeleton also undergoes substantial structural changes during the course of reproduction. Lactation induces dramatic maternal bone loss at extremely high rates of up to 1% decrease in bone mineral density (BMD) per month of lactation [4-7], and maternal bone mass may also decline during pregnancy [8]. Following weaning, multiple clinical and preclinical studies have demonstrated that reproductive bone changes undergo a period of recovery, where the maternal skeleton enters an anabolic phase, with a positive balance towards bone formation, resulting in a significant increase in bone mass [9-13].

In spite of the impressive period of recovery that occurs post-weaning, the long-term effects of reproduction on maternal bone structure remain unclear. Although the majority of clinical studies indicate that BMD recovers within one year of weaning [14], recent clinical evaluations of recovery of the trabecular microarchitecture have demonstrated that reproduction-induced deteriorations in trabecular microstructure persist for at least 18-43 months post-partum

[15,16]. Furthermore, rodent studies have demonstrated that substantial microarchitectural impairments in the trabecular bone compartment remain long after weaning at several skeletal sites [10,17-19]. In contrast, a large number of epidemiological studies, summarized by Kovacs [14], have evaluated the impact of pregnancy and/or lactation on long-term risk of fracture or osteoporosis, and the vast majority indicated that reproductive history has no adverse, or even a protective effect on postmenopausal risk of osteoporosis/fracture [14].

Taken together, the current literature suggests that reproduction induces permanent alterations in maternal bone microarchitecture but has a protective effect against postmenopausal fracture risk, thereby forming a paradox. To better understand these conflicting findings, our previous study developed a rat model to precisely track the effects of reproduction over the long-term. Our findings indicated a significant increase in cortical bone size at the proximal tibia in reproductive rats, which may mask permanent alterations in trabecular microstructure [19]. Adaptations of cortical bone may also explain the complete post-weaning recovery of BMD reported in clinical studies [14], as areal BMD is unable to distinguish between the trabecular and cortical compartments.

Although cortical bone adaptations may be able to compensate for irreversible deterioration of trabecular microstructure at some sites, at other locations, trabecular bone has a critical load-bearing function. In addition, postmenopausal bone loss further impacts both trabecular and cortical structure and the effects of the reproduction-induced alterations in skeletal microarchitecture on postmenopausal bone loss patterns remain unknown. The current study aimed to investigate the effects of reproduction and lactation on skeletal responses to estrogen deficiency later in life. Using a rat model, combined with *in vivo* micro-computed tomography (μCT) imaging and bone histomorphometry, we tracked the changes in bone structure and

cellular activities in response to estrogen deficiency following ovariectomy (OVX) surgery in animals with and without a reproductive history. We hypothesized that long-term, reproduction-induced alterations in bone microarchitecture and cellular activities may result in distinct patterns of estrogen-deficiency-induced bone loss and may exert protective effects on bone's mechanical competence after OVX. In this paper, we will refer to the rats without a history of reproduction as "*virgin rats*" and the rats with a history of reproduction as "*reproductive rats*".

2. Methods:

2.1 Animal Protocol:

All animal procedures were approved by the University of Pennsylvania's Institutional Animal Care and Use Committee. Four separate sets of animal experiments were performed in rats with and without a history of reproduction: 1.) to track longitudinal changes in bone structure at the proximal tibia post-OVX, 2.) to quantify bone cell numbers and surfaces following OVX, 3.) to quantify bone resorption and formation activities following OVX, and 4.) to compare the effects of OVX on bone structure and mechanics at the lumbar vertebra and femur midshaft. All rats were purchased from Charles River at 3 months of age, and were randomly assigned to one of two groups: reproductive and virgin. Starting at age 4 months, rats in the reproductive group underwent two to three reproductive cycles, each consisting of pregnancy (3 weeks), lactation (3 weeks), and post-weaning recovery (3-6 weeks). In order to ensure consistent suckling intensity, litter sizes were normalized to 8-9 pups per mother within the first 48 hours after birth. All rats were fed a high calcium diet (LabDiet 5001 Rodent Diet, LabDiet, St. Louis, MO, USA; 0.95% Ca) throughout the experiment. Rats were housed in standard conditions in groups of 3 rats per cage throughout the experiment, with two exceptions: reproductive rats were separated to 1 rat per cage during the last week of pregnancy and

remained separated throughout the lactation period, and all rats that underwent OVX surgery were separated to 1 rat per cage for two weeks following surgery. Rats were euthanized at age 14-19 months.

2.2 Longitudinal Tracking of Post-OVX Changes in Bone Microstructure at the Proximal Tibia

Twenty-four rats (12 reproductive, 12 virgin) were used for this experiment. At age 12 months, after 3 repeated cycles of pregnancy and lactation in the reproductive group, all rats underwent ovariectomy (OVX) surgery to induce estrogen deficiency. Rats received *in vivo* μCT scans of the proximal tibia immediately prior to OVX, as well as 4, 8, and 12 weeks post-OVX, and all rats were euthanized at 12 weeks post-OVX (age 15 months). The uterus was collected and weighed immediately post-sacrifice to confirm the success of OVX surgery. One rat died during the pre-OVX μCT scan, 4 rats died from complications of OVX surgery, and 2 OVX surgical procedures were deemed unsuccessful (based on uterus weight), resulting in a final sample size of n=9 in the reproductive group, and n=8 in the virgin group.

2.2.1 In Vivo μCT Scans:

In vivo μCT imaging (Scanco vivaCT40, Scanco Medical AG, Brüttisellen, Switzerland) of the right proximal tibia was performed at 0, 4, 8, and 12 weeks post-OVX, following the protocol described in [20]. Briefly, rats were anesthetized (4/2% isoflurane), and the right tibia was inserted into a customized holder to ensure minimal motion. A 4.2 mm thick segment of the proximal tibia, located immediately distal to the proximal growth plate, was imaged at 10.5 μm voxel size, resulting in a radiation dose of 0.639 Gy and a total scan time of 20 minutes. All scans were made using 200 ms integration time, 145 μA current, and 55 kVp energy.

2.2.2 Trabecular and Cortical Bone Microstructural Analysis:

Image registration was performed to identify a consistent volume of interest (VOI) so that changes in trabecular microstructure within the sequential *in vivo* μCT images could be quantified. Using a mutual-information-based, landmark-initialized, open-source registration toolkit (National Library of Medicine Insight Segmentation and Registration Toolkit), *in vivo* μCT images made for each rat at 0, 4, 8, and 12 weeks post-OVX were aligned to each other. As described in [20], a 1.5-mm thick, trabecular VOI, located 2.5 mm distal to the growth plate, was identified in the week 12 scan, and translated back to earlier scans made at weeks 0, 4, and 8 post-OVX using the transformation matrices that resulted from the registrations. All VOIs were visually inspected to ensure accurate identification of a consistent trabecular region.

Standard parameters of trabecular bone microstructure [21] were measured within each trabecular VOI at the proximal tibia. Briefly, images of trabecular bone were filtered and thresholded through application of a Gaussian filter (sigma=1.2, support=2), followed by a global threshold corresponding to 565 mgHA/cm^3 (threshold identified using an adaptive threshold function provided by the μCT scanner manufacturer). Trabecular microstructure was then quantified based on standard parameters: bone volume fraction (BV/TV), trabecular number (Tb.N), trabecular thickness (Tb.Th), trabecular separation (Tb.Sp), structure model index (SMI), and connectivity density (Conn.D).

To evaluate cortical bone microstructure at the proximal tibia, a 50-slice thick cortical VOI located 3.5 mm distal to the growth plate was identified using a semi-automated segmentation procedure similar to that described in [22]. Voxels within the cortical VOI were then filtered (Gaussian filter, sigma=1.2, support=2), and thresholded by application of a global threshold corresponding to 709 mgHA/cm^3. Standard parameters of cortical bone microstructure,

including cortical area (Ct.Area), cortical thickness (Ct.Th), periosteal perimeter (P.Perim), endosteal perimeter (E.Perim), and polar moment of inertia (pMOI), were measured.

2.2.3 Micro-Finite Element Analysis (μFEA)

A 1.5 mm-thick region of the proximal tibia located 2.5 mm distal to the growth plate, including both cortical and trabecular bone compartments, was isolated from the μCT image. Images were downsampled to a voxel size of 15.75 μm to construct a finite element model. Each bone voxel was converted to an eight-node brick element, and bone was modeled as a linear elastic material with Young's modulus of 15 GPa and Poisson's ratio of 0.3 [(23)]. An axial compression was simulated by applying a displacement of 0.01 mm, and the resulting reaction force was calculated as described in [(24)]. The reaction force was then divided by the displacement to estimate whole-bone stiffness of the proximal tibia.

2.2.4 Linear Regression Analysis

To test whether the degree of post-OVX bone loss is influenced by the baseline trabecular bone microarchitecture, correlations between baseline trabecular microstructure and the degree of post-OVX bone loss were evaluated using linear regression. Subsequently, a stepwise multiple linear regression analysis was performed to identify the most important and independent predictors of post-OVX bone loss.

2.2.5 Individual Trabecular Dynamics Analysis

In vivo μCT images of the proximal tibia made at weeks 0 and 4 post-OVX were used to assess the effects of reproductive history on the post-OVX deterioration of individual trabecular elements. For each rat, sequential μCT images were registered to precisely align the trabecular features, as described in [(20,25,26)], and a 1.5x1.5x1 mm trabecular subvolume located 1 mm distal to the growth plate was extracted from μCT images at 0 and 4 weeks post-OVX. The post-OVX

changes of each individual trabecula, such as percent bone loss due to trabecular thinning, rod disconnection, or plate perforation, were quantified through an individual trabecular dynamics (ITD) analysis, as described in [27]. Trabeculae from all virgin or reproductive rats were pooled together, resulting in a total of 4,752 trabeculae in the virgin and 1,564 trabeculae in the reproductive group. Histogram analysis was performed for each group to categorize the trabeculae into 9 thickness bins, and the mean percent bone loss of trabeculae in each thickness bin was calculated for both virgin and reproductive groups.

2.3 Evaluation of Bone Cell Activities Pre- and Post-OVX

A total of 35 rats were used for this experiment.18 rats (10 reproductive, 8 virgin) underwent OVX surgery at age 12 months, after 3 repeated cycles of pregnancy and lactation in the reproductive group. One rat died from surgical complications, resulting in a final sample size of n=9 in the reproductive OVX group, and n=8 in the virgin OVX group. At 4 weeks post-OVX, all rats were euthanized. In addition, age-matched reproductive (n=7) and virgin (n=10) intact rats that did not undergo OVX surgery were used as an estrogen-replete control group. For all rats, right proximal tibiae were harvested immediately after sacrifice and embedded in methyl methacrylate (MMA) for un-decalcified histology. A Polycut-S motorized microtome (Reichert, Heidelberg, Germany) was then used to obtain 5 μm-thick sections. Sections were stained with Goldner's trichrome, and osteoblast number (N.Ob/BS), osteoclast number (N.Oc/BS), osteoblast surface (Ob.S/BS), and osteoclast surface (Oc.S/BS) were measured in the secondary spongiosa using OsteoMeasure Software (OsteoMetrics, Inc., Decatur, GA).

2.4 Evaluation of Bone Remodeling Dynamics Pre- and Post-OVX

A total of 39 rats were used for this set of experiments. The first experiment consisted of 24 rats (12 reproductive, 12 virgin). Half of these rats (6 reproductive, 6 virgin) underwent OVX

surgery at age 10 months, after 2 repeated cycles of pregnancy and lactation in the reproductive group. At 8 weeks post-OVX, all rats were euthanized. The remaining rats (6 reproductive, 6 virgin) that did not undergo OVX surgery, were used as an estrogen-replete controls. All rats received subcutaneous injections of calcein (20 mg/kg, Sigma-Aldrich, St. Louis, MO) at 11 days prior to sacrifice, and intraperitoneal injections of alizarin complexone (30mg/kg, Sigma-Aldrich, St. Louis, MO) at 2 days prior to sacrifice. The right proximal tibiae were harvested immediately after sacrifice and embedded in MMA. Two samples were damaged during MMA embedding, resulting in a final sample size of n=4 in the reproductive Intact group, and n=6 in the virgin Intact, reproductive OVX, and virgin OVX groups. Dynamic bone histomorphometry was performed on 8 μm-thick MMA sections. Bone formation rate (BFR/BS), mineral apposition rate (MAR), and mineralizing surfaces (MS/BS) were measured in the secondary spongiosa of the proximal tibia using OsteoMeasure Software (OsteoMetrics, Inc., Decatur, GA).

In the second experiment, 15 rats (8 reproductive, 7 virgin) underwent OVX surgery at age 10 months, after 2 repeated cycles of pregnancy and lactation in the reproductive group. Blood was collected via tail vein at 0 and 14 days post-OVX and serum levels of bone formation marker P1NP were determined (Rat/Mouse P1NP Enzyme Immunoassay, Immunodiagnostic Systems Inc, UK). Blood was also collected via tail vein at 0 and 7 days post-OVX in the virgin OVX (n=8) and reproductive OVX (n=9) groups described in Section 2.3. Serum levels of bone resorption marker TRAcP 5b (TRAP) were determined (RatTRAP^{TM} Assay, Immunodiagnostic Systems Inc, UK). Fold changes post- OVX were calculated for both serum P1NP and TRAP.

2.5 Cross-Sectional Comparison of the Effects of OVX and Reproductive History on Bone Microstructure and Mechanical Properties at Multiple Skeletal Sites

Reproductive and virgin post-OVX rats described in Section 2.2 were used for this portion of the experiment. In addition, age-matched reproductive (n=8) and virgin (n=10) intact rats that did not undergo OVX surgery were used as an estrogen-replete control group. All rats were sacrificed at age 15-19 months. The right femur and the second and fourth lumbar vertebrae (L2 and L4) were harvested from each rat.

2.5.1 Ex Vivo μCT Scans:

The right femur midshaft and L4 vertebra were imaged after sacrifice. A 2.1 mm thick section of the femur midshaft (located at the midpoint between the end of the distal epiphysis and the bottom of the femoral head), and a 6.3 mm thick section of the center of the L4 vertebral body, were acquired at 10.5 μm voxel size. A VOI was manually identified to include all trabecular bone and exclude the cortex in the center 2 mm of the L4 vertebral body. At the femur midshaft, a 0.5 mm thick cortical VOI was identified at the midpoint between the distal epiphysis and femoral head. Images were then Gaussian filtered (sigma=1.2, support=2), and a global threshold corresponding to 565 mgHA/cm^3 for the vertebra and 772 mgHA/cm^3 for the femur midshaft was applied. Standard parameters of trabecular microarchitecture at the vertebra, and cortical bone structure at the femur midshaft, were measured.

2.5.2 Mechanical Testing:

The right femur and L2 vertebra were cleaned of soft tissue and were tested to failure using a standard mechanical testing device (Instron 5542, Norwood, MA).Femurs were tested in three-point bending, by applying a displacement rate of 1.8 mm/minute until failure. L2 vertebrae were prepared for uniaxial compression testing by using a procedure modified from [28]. A section of the center 60% of the vertebral body was isolated by removing the processes and making two parallel cuts at the cranial and caudal ends of the vertebral body. The resulting

specimen was placed between two parallel platens and was compressed to failure at a displacement rate of 1.8 mm/minute. For both the femur and lumbar vertebrae, peak load, stiffness, and energy to failure were determined based on the load-displacement curves generated from mechanical testing.

2.6 Statistical Analysis

All results are reported as mean ± standard deviation. Longitudinal comparisons of bone parameters pre-OVX and 12 weeks post-OVX at the proximal tibia were made using 2-way analysis of variance (ANOVA), to compare the effects of reproductive history and time post-OVX. In the presence of a statistically significant interaction effect, group-wise comparisons were evaluated using Bonferroni *post hoc* corrections. Cross-sectional comparisons of bone cell activities, bone remodeling dynamics, and bone microstructure and mechanical properties of femoral and vertebral bone between virgin and reproductive groups and between intact and OVX groups were made using Student's t-tests with Bonferroni corrections for multiple comparisons. For all tests, a two-tailed p-value below 0.05 was considered to indicate statistical significance. In the presence of significant differences, the degree of variation between groups is reported as the percent difference, for all parameters except SMI. SMI ranges from -3 to 3; therefore, inter-group differences in SMI are reported as the absolute difference.

3. Results:

3.1 Rats with a reproductive history show altered trabecular and cortical microstructure and undergo a reduced rate of post-OVX trabecular bone loss at the proximal tibia

After 3 cycles of reproduction, reproductive rats showed altered trabecular microarchitecture at the proximal tibia, relative to virgins (Figure 1A-H). Reproductive rats had 49% lower BV/TV, 50% lower Tb.N, 127% higher Tb.Sp, and 77% lower Conn.D than virgins,

but had 13% greater Tb.Th. Over the 12-week post-OVX period, virgin rats underwent dramatic 76%, 52%, and 87% reductions in BV/TV, Tb.N, and Conn.D, respectively, and underwent an increase in SMI of 1.47. In contrast, reproductive rats underwent a substantially lower degree of trabecular deterioration post-OVX, showing a 53% decrease in BV/TV and no significant change in any other microstructural parameters. OVX had no effect on Tb.Th in either group. By 12 weeks post-OVX, there were no remaining differences between reproductive and virgin rats in BV/TV, Tb.N, Conn.D, and SMI. However, reproductive rats continued to show a 20% elevated Tb.Sp and 17% greater Tb.Th compared to virgins.

In addition to baseline differences in trabecular bone, reproductive and virgin rats also showed substantial differences in cortical bone microarchitecture at the proximal tibia prior to OVX (Figure 1I-M). Compared to virgins, reproductive rats had 22% greater pMOI, indicating a greater structural resistance to bending. This appeared to result from a more robust cortical bone structure in the reproductive group, as reproductive rats also had 10% greater cortical Ct.Area, 7% greater Ct.Th, and 8% and 4% greater E.Perim and P.Perim, respectively, than virgin rats. OVX induced no changes in cortical bone structure in both virgin and reproductive rats. Thus, at 12 weeks post-OVX, reproductive rats continued to have 22%, 13%, 12%, 6%, and 3% greater pMOI, Ct.Area, Ct.Th, E.Perim, and P.Perim, respectively, as compared to virgins.

Prior to OVX, both virgin and reproductive rats had an average whole-bone stiffness of 45-50 kN/mm at the proximal tibia, with no differences between the two groups (Figure1N). Over the 12-week period following OVX, virgin rats underwent a 22% decrease in whole-bone stiffness, while reproductive rats showed no change in stiffness. As a result of these distinct patterns of post-OVX changes, by 12 weeks post-OVX, virgin rats had a substantial, 13% lower whole-bone stiffness at the proximal tibia as compared to the reproductive group.

3.2 Bone cell activities and bone remodeling dynamics are not affected by reproductive history

Static and dynamic bone histomorphometry (Figure 2) demonstrated that, in post-OVX virgin rats, Ob.N/BS, Ob.S/BS, and MS/BS were 32%, 37%, and 59% elevated, respectively, as compared to intact virgins. Regardless of reproductive history, Oc.N/BS was 52% elevated at 4 weeks post-OVX. Additionally, Oc.S/BS was 88% elevated at 4 weeks post-OVX in reproductive rats. Serum level of TRAP increased 1.9 and 3.2 folds 1 week post-OVX in virgin and reproductive rats, respectively. Moreover, serum level of P1NP increased 2.1 and 2.3 folds 2 weeks post-OVX in virgin and reproductive rats, respectively. However, in both intact and OVX rats, there were no significant reproductive-history-based differences in measures of bone cell activities or bone remodeling dynamics. Furthermore, there were no significant reproductive-history-based differences in fold changes in serum levels of P1NP or TRAP in response to OVX.

3.3 Baseline trabecular microstructure is correlated to the post-OVX bone loss rate

Linear regression was performed to evaluate the relationship between baseline parameters of trabecular microstructure and the percent decrease in BV/TV over the 12-week post-OVX period. Baseline BV/TV, Tb.N, Tb.Th, Tb.Sp, and Conn.D were all significantly correlated with the extent of post-OVX bone loss, with r^2 values ranging from 0.32 to 0.60 (Figure 3). The effects of baseline trabecular surface area (BS) and surface area-to-volume ratio (BS/BV) on post-OVX bone loss were also investigated. Baseline BS was found to be moderately correlated to the extent of post-OVX bone loss, with an r^2 value of 0.28, while no significant correlation was found between baseline BS/BV and the percent decrease in BV/TV post-OVX. Stepwise multiple linear regression was performed to further identify which combination of baseline trabecular parameters was most predictive of the degree of post-OVX bone loss. The

combination of baseline Tb.Th and Tb.N was found to be most strongly associated with the percent decrease in BV/TV, with an adjusted r^2 value of 0.69.

3.4 The extent of post-OVX microstructural deterioration is highly dependent on baseline trabecular thickness

Individual trabecular segmentation (ITS) analysis [29] was applied to isolate individual trabecular rod-like and plate-like elements, and changes in the volume, thickness, and connectivity of each trabecula over the first 4 weeks post-OVX were tracked through individual trabecular dynamics (ITD) analysis [27] (Figure 4A). Consistent with microstructural findings, virgin rats underwent a substantially higher rate of bone loss over the first 4 weeks post-OVX than reproductive rats (Figure 4B). In addition to differences in the overall rate of post-OVX bone loss, reproductive and virgin rats also showed variations in the microstructural mechanisms responsible for the bone loss. In virgin rats, 20% of post-OVX bone loss resulted from connectivity deterioration (rod disconnection or plate perforation), while 80% of bone loss resulted from alternate mechanisms, such as trabecular thinning, that do not impact the microarchitecture/connectivity (Figure 4B). In contrast, in reproductive rats, a much smaller proportion of only 11% of post-OVX bone loss was caused by deteriorated connectivity, whereas 89% of bone loss did not impact the trabecular microarchitecture. This lower rate of connectivity deterioration in the reproductive group was highly consistent with microstructural findings, which indicated that, in contrast to virgins, reproductive rats underwent minimal changes in Tb.N or Conn.D following OVX.

Further investigation into the baseline characteristics of individual trabecular elements indicated that the trabeculae undergoing connectivity deterioration, were significantly thinner than those that remained intact after OVX (Figure 4C). This was true in both the reproductive

and virgin groups. Furthermore, a histogram analysis, where trabeculae were binned into 9 groups based on their baseline thickness, indicated that thinner trabeculae underwent a greater percentage of bone loss (Figure 4D&E). In both virgin and reproductive groups, the baseline thickness particularly affected the degree of post-OVX bone loss of trabecular elements that were less than 0.06 mm thick, as there were significant differences among thickness bins in the percent bone loss for all thickness bins below 0.06 mm. The effect of trabecular thickness on post-OVX bone loss plateaued for thicknesses greater than 0.06 mm, as a further increase in thickness beyond 0.06 mm did not lead to further reduction in bone loss. In addition, within each thickness bin, the trabeculae of reproductive rats underwent significantly less bone loss when compared to those of virgin rats (Figure 4D&E). This finding was consistent across all 9 thickness groups.

3.5 Reproductive history induces long-lasting alterations in trabecular microarchitecture at the lumbar vertebra, but minimally affects cortical microstructure at the femur midshaft or whole-bone vertebral or femoral mechanical properties

Intact reproductive rats had 31% lower BV/TV, 23% lower Tb.N, 34% higher Tb.Sp, 32% lower Conn.D, and an increased SMI of 0.76 than intact virgin rats at the lumbar vertebra. Twelve weeks after OVX surgery, there was no longer a difference between virgin and reproductive rats in BV/TV and SMI. However, reproductive rats still had 19% and 34% lower Tb.N and Conn.D and 23% greater Tb.Sp when compared to virgins (Figure 5).

Intact reproductive rats had 13% greater E.Perim at the femur midshaft than virgin rats. There were no reproductive history-based differences in any other microstructural parameters at the femur midshaft (Figure 6).

Reproductive history had no effect on whole-bone mechanics at both the lumbar vertebra and femur midshaft, as the peak load, stiffness, and energy to failure were not different among groups at either site (Figures 5I-K and 6F-H).

4. Discussion:

This study evaluated the impact of a history of pregnancy and lactation on estrogen deficiency-induced bone loss patterns. Taken together, results indicate that, although a reproductive history caused permanent alterations in trabecular and cortical bone microarchitecture, rats with a reproductive history also underwent substantially altered patterns of bone loss after OVX, and as a result, by 12 weeks post-OVX, there were no remaining adverse effects of reproductive history on bone microstructure at the tibia. Furthermore, our findings also suggest that reproductive history-based differences in the rate of post-OVX bone loss are partially due to alterations in the baseline trabecular microarchitecture prior to OVX. In particular, the baseline Tb.Th was found to be highly predictive of the rate of post-OVX bone loss and connectivity deterioration.

Prior to OVX, reproductive rats had substantially different trabecular as well as cortical microarchitecture at the proximal tibia compared to virgins, confirming the long-lasting effects of reproduction on maternal bone. Consistent with our previous study [19], BV/TV, Tb.N, and Conn.D were reduced, and Tb.Th, pMOI, Ct.Area, Ct.Th, E.Perim, and P.Perim were elevated, at the proximal tibia after three reproductive cycles. This finding agrees with the previously reported incomplete recovery of trabecular microarchitecture following pregnancy/lactation [9,16-18,30-32], and is also consistent with a recent study suggesting that a long duration of lactation is associated with long-term elevations in the cross-sectional moment of inertia of the tibial cortical bone [33].

In addition to differences in bone microarchitecture prior to OVX, rats with and without a reproductive history also showed substantial variations in the pattern of post-OVX bone loss at the proximal tibia. While both groups of rats underwent substantial decreases in BV/TV, reproductive rats had no significant post-OVX changes in trabecular microarchitecture, while virgins showed a dramatic decrease in the number, connectivity, and plate-like character of the trabeculae. These findings in virgin rats are highly consistent with previous *in vivo* μCT-based evaluations of post-OVX changes in trabecular bone microarchitecture at the rat proximal tibia [34,35]. As a result of the lower degree of post-OVX bone loss in the reproductive group, reproductive and virgin rats had a similar trabecular microstructure by 12 weeks post-OVX, despite differences between the two groups at baseline. These findings demonstrated altered rates of post-OVX bone loss between virgin and reproductive groups, which may help to explain the clinical paradox that reproductive history does not adversely affect postmenopausal BMD [14] in spite of its long-lasting skeletal effects [16,30,32]. In addition to its effects on bone structure/volume, the greater rate of bone loss observed in virgin rats may directly affect fracture risk, as a high rate of bone loss after menopause has been found to confer an equally high risk of future fracture as does a low baseline bone mass [36].

In contrast to trabecular bone, both reproductive and virgin rats showed no post-OVX changes in cortical bone microstructure at the tibia. By comparison, a previous study tracking post-OVX changes at the rat tibial metaphysis indicated increased Ct.Th starting at 14 weeks post-OVX [34]. However, post-OVX changes in cortical bone structure occur much more slowly and take longer to develop than changes in trabecular microarchitecture [37], possibly explaining the lack of changes in cortical microstructure observed in the current study, which only followed rats up to 12 weeks post-OVX.

Taken together, the combined effects of OVX on tibial trabecular and cortical microarchitecture in rats with and without a reproductive history led to interesting patterns of post-OVX deterioration of whole-bone stiffness. While reproductive rats showed no change in whole-bone stiffness following OVX, the stiffness of virgin rat tibiae decreased significantly, leading to lower stiffness in this group at 12 weeks post-OVX compared to the reproductive group, despite no difference between the two groups at baseline. This suggests that in virgin rats, the post OVX trabecular deteriorations were substantial enough to cause a reduction in stiffness in spite of no changes in cortical bone structure. On the other hand, the relatively constant whole-bone stiffness in the reproductive group post-OVX in spite of mild reductions in trabecular bone volume may be the result of long-term adaptations in cortical bone microstructure that occurred over the course of multiple reproductive cycles [19], which may compensate for deteriorations in trabecular microarchitecture.

To better understand mechanisms behind the variable rates of post-OVX trabecular bone loss between reproductive and virgin rats, we evaluated the bone cell activities and bone remodeling dynamics at the proximal tibia. Compared to intact animals, post-OVX rats showed elevations in osteoblast and osteoclast numbers and/or surface areas, serum markers of bone resorption and formation, and mineralizing surface. However there were no reproductive history-based differences in bone cell numbers and surface and bone remodeling activities in either the intact or post-OVX groups, suggesting that an alternate mechanism, beyond differences in osteoblast/osteoclast numbers or surfaces, may be responsible for the disparate patterns of post-OVX bone loss observed in virgin and reproductive rats

One factor which may impact the trabecular bone loss rate independently of cell activities is the baseline microarchitecture. For instance, computational simulation studies [38,39], as well as

a cross-sectional clinical evaluation [40], have suggested that the bone loss rate may be affected by the surface area of the bone that is available for osteoblasts/osteoclasts to act upon. Consistent with this hypothesis, a recent longitudinal evaluation of perimenopausal bone loss patterns found that changes in bone mass and structure at the femoral neck varied depending on baseline bone size, where women with a wider femoral neck at baseline undergoing a greater postmenopausal reduction in bone mass [41]. This was hypothesized to be due, in part, to differences in the baseline porosity among women with different skeletal phenotypes, as greater cortical width was shown to be associated with elevated porosity [42], which would allow for a larger surface area upon which bone remodeling could take place, possibly resulting in an elevated rate of postmenopausal bone loss [41]. To evaluate the relationship between baseline parameters of trabecular microarchitecture and the post-OVX bone loss rate in the current study, a linear regression analysis was performed. Although many baseline parameters of trabecular microstructure were significantly correlated to the post-OVX bone loss rate, multiple linear regression analysis indicated that Tb.N and Tb.Th were the most strongly associated with the rate of bone loss. Contrary to what was expected based on previous computational simulation-based evaluations [38,39], the degree of post-OVX bone loss had no correlation with the baseline bone surface area-to-volume ratio, suggesting that the baseline trabecular microarchitecture impacted the rate of bone loss independently of its effect on surface area.

Several studies have indicated that in addition to the metabolic bone remodeling deficit, where bone loss occurs due to increased activity of osteoclasts relative to osteoblasts, another significant contributor to osteoporotic bone loss is microstructural deterioration, where perforated trabeculae and separations of trabeculae from the surrounding structure lead to an accelerated bone loss [43-45]. These findings, together with our results that the baseline trabecular

thickness was inversely correlated to the degree of post-OVX bone loss, suggest that a trabecular microstructure consisting of thin trabeculae that are easily perforated or separated may contribute to microstructural deterioration, and conversely, that thicker trabeculae may be protective against post-OVX trabecular connectivity deterioration and bone loss (Figure 4F). Indeed, our results from ITD analysis of over 6,000 individual trabeculae have demonstrated that in both reproductive and virgin rats, thicker trabeculae underwent a significantly reduced bone loss rate compared to thin trabeculae. Furthermore, in virgin rats, which had a larger population of thin trabeculae, a substantially larger proportion of post-OVX bone loss resulted from connectivity deterioration than in reproductive animals. This is likely due to the increased susceptibility of thin trabeculae to undergo perforation or separation as a result of elevated bone remodeling [43] (Figure 4F). Thus, the existence of a larger proportion of thick trabeculae in the reproductive group partially explains the protective effect of reproductive history on post-OVX bone loss. Furthermore, in a follow-up study, we tracked post-OVX bone loss patterns in a homogeneous population of 62 virgin rats over the first 4 weeks following OVX [46]. This study eliminated any possible confounding effects of reproductive history and therefore allowed the effect of baseline trabecular microarchitecture on post-OVX bone loss to be evaluated independently. Results confirmed our findings in reproductive rats that thicker trabeculae underwent a significantly lower degree of post-OVX bone loss, suggesting that a trabecular bone phenotype with thicker trabeculae may be protective against estrogen-deficiency-induced bone loss.

Studies investigating the effects of pregnancy, lactation, and weaning at multiple skeletal sites have indicated that these processes affect the bone in a highly site-specific manner [18,47]. In addition to the proximal tibia, we investigated the effects of reproductive history on post-OVX bone loss at the lumbar vertebra and femur midshaft. However, results were less clear at these

skeletal sites. At the lumbar vertebra, trabecular bone volume and microstructure were significantly different between virgin and reproductive animals. These differences were reduced by 12 weeks after OVX, as BV/TV and SMI were no longer different between the virgin and reproductive animals at this time point. However, at 12 weeks post-OVX, reproductive rats still had fewer, more separated and disconnected trabeculae than virgins, and minimal effects of OVX status on vertebral trabecular microstructure were observed. In addition, minimal differences were observed between groups at the femur midshaft. In contrast to the rat tibia, which loses bone rapidly for the first 3 months following OVX before the trabecular structure stabilizes, the lumbar vertebra loses bone much more gradually after OVX, and does not reach a steady state until 9 months post-surgery [37,48,49]. Post-OVX changes at the femur midshaft may take even longer to detect than those at the lumbar vertebra, as structural and mechanical changes at the rat femur midshaft are reported to be measureable only after 6-9 months post-OVX [37]. Therefore, the timeframe of this study, which was selected to optimize the precise tracking of post-OVX changes at the proximal tibia, may have been insufficient to allow for evaluations of the effects of reproductive history on post-OVX changes at other skeletal sites. Future investigations, including a longer post-OVX monitoring period, will be required to confirm whether or not reproductive history impacts post-OVX changes at the femur and lumbar vertebra.

The current study mainly focuses on the microstructural properties that influence post-OVX bone loss patterns in rats with and without a reproductive history. However, many other aspects of bone properties, *e.g.*, at the cellular or molecular level, may have been significantly altered during reproduction, and may also affect the skeletal response to estrogen deficiency later in life. Our results showed that even at the same baseline trabecular thickness, the trabeculae of

reproductive rats underwent a significantly lower rate of bone loss than those of virgin rats (Figure 4D &E), suggesting that additional factors beyond baseline trabecular thickness may also protect reproductive bone from OVX bone loss. To fully understand the mechanisms behind this protective effect, further investigation is required.

Overall, this study demonstrates that, in addition to its direct effects on trabecular and cortical bone microarchitecture, a history of reproduction also results in an altered skeletal response to estrogen-deficiency-induced bone loss later in life. Compared to virgins, rats with a reproductive history had lower trabecular bone mass, altered trabecular microarchitecture, and a more robust cortical structure at the proximal tibia prior to OVX. However, as a result of the lower rate of post-OVX trabecular bone loss in the reproductive group, by 12 weeks post-OVX, there were no remaining deficits in trabecular microarchitecture in reproductive rats, while this group continued to show elevated trabecular thickness and increased robustness of cortical bone, resulting in greater bone stiffness, relative to virgins. Further evaluation suggested that reproductive-history-induced differences in OVX response did not result from alterations in bone cell activities or bone turnover, but instead were likely due to differences in baseline trabecular microstructure, and in particular, trabecular thickness. Taken together, these findings indicate that reproductive history modulates the skeletal response to OVX-induced estrogen deficiency, resulting in a greater whole-bone stiffness in reproductive rats after OVX, which may explain, in part, how pregnancy/lactation are able to induce long-lasting alterations in maternal bone microstructure without adversely affecting, and possibly even protecting against postmenopausal risk of osteoporosis or fracture.

5. Acknowledgements:

Research reported in this publication was supported by the Penn Center for Musculoskeletal Diseases (PCMD) NIH/NIAMS P30-AR069619, NIH/NIAMS R03-AR065145 (to XSL), NIH/NIAMS K01-AR066743 (to XSL), NIH/NIAMS R01-AR071718 (to XSL), National Science Foundation (NSF) Award #1653216 (to XSL), and NSF Graduate Research Fellowship (to CMJdB). We'd like to thank Casey Krickus for technical assistance on trabecular bone analysis.

6. Authors' roles:

Study design: XSL, CMJdB. Study conduct: CMJdB, YL, LL, HZ, WJT, TL, WT. Data collection: CMJdB, YL, LL, HZ, WJT. Data analysis: CMJdB, YL, LL, HZ, WJT. Data interpretation: XSL, CMJdB. Drafting manuscript: CMJdB, XSL. Revising manuscript content: YL, LL, HZ, WJT, TL, WT, LQ. Approving final version of manuscript: XSL, CMJdB, YL, LL, HZ, WJT, TL, WT, LQ. XSL and CMJdB take responsibility for the integrity of the data analysis.

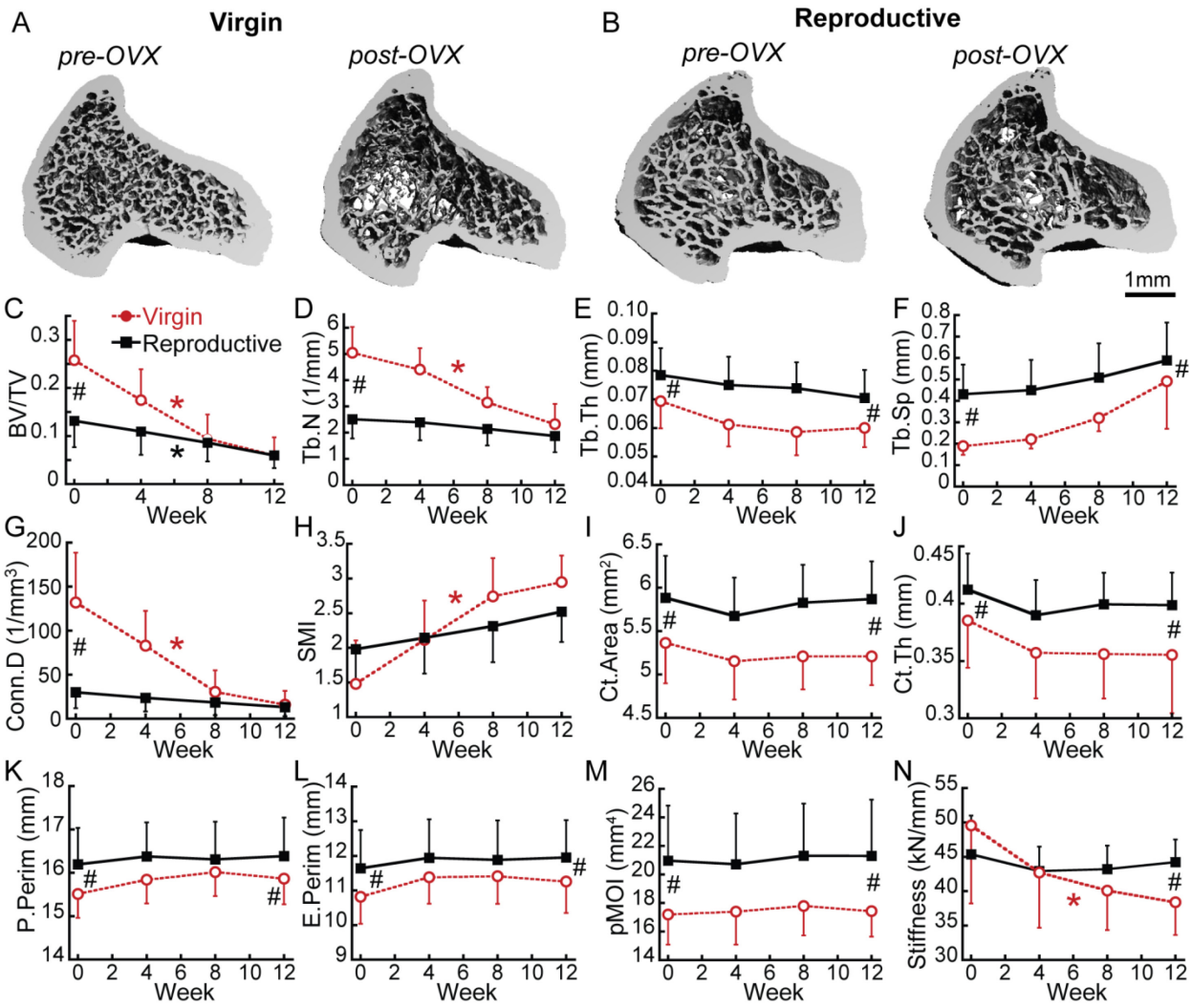

Figure 1. (A-B) Representative 3D renderings illustrating the effects of OVX on trabecular bone at the proximal tibia in (A) virgin and (B) reproductive rats. (C-H) Post-OVX changes in trabecular bone microstructure, including (C) BV/TV, (D) Tb.N, (E) Tb.Th, and (F) Tb.Sp, (G) Conn.D, and (H) SMI. (I-M) Post-OVX changes in cortical bone microstructure, including (I) Ct.Area, (J) Ct.Th, (K) P.Perim, (L) E. Perim, and (M) pMOI. (N) Post-OVX changes in FEA-derived whole-bone stiffness. #: significant difference between reproductive and virgin rats at week 0 or week 12 post-OVX ($p<0.05$). *: significant change over the 12-week post-OVX period ($p<0.05$).

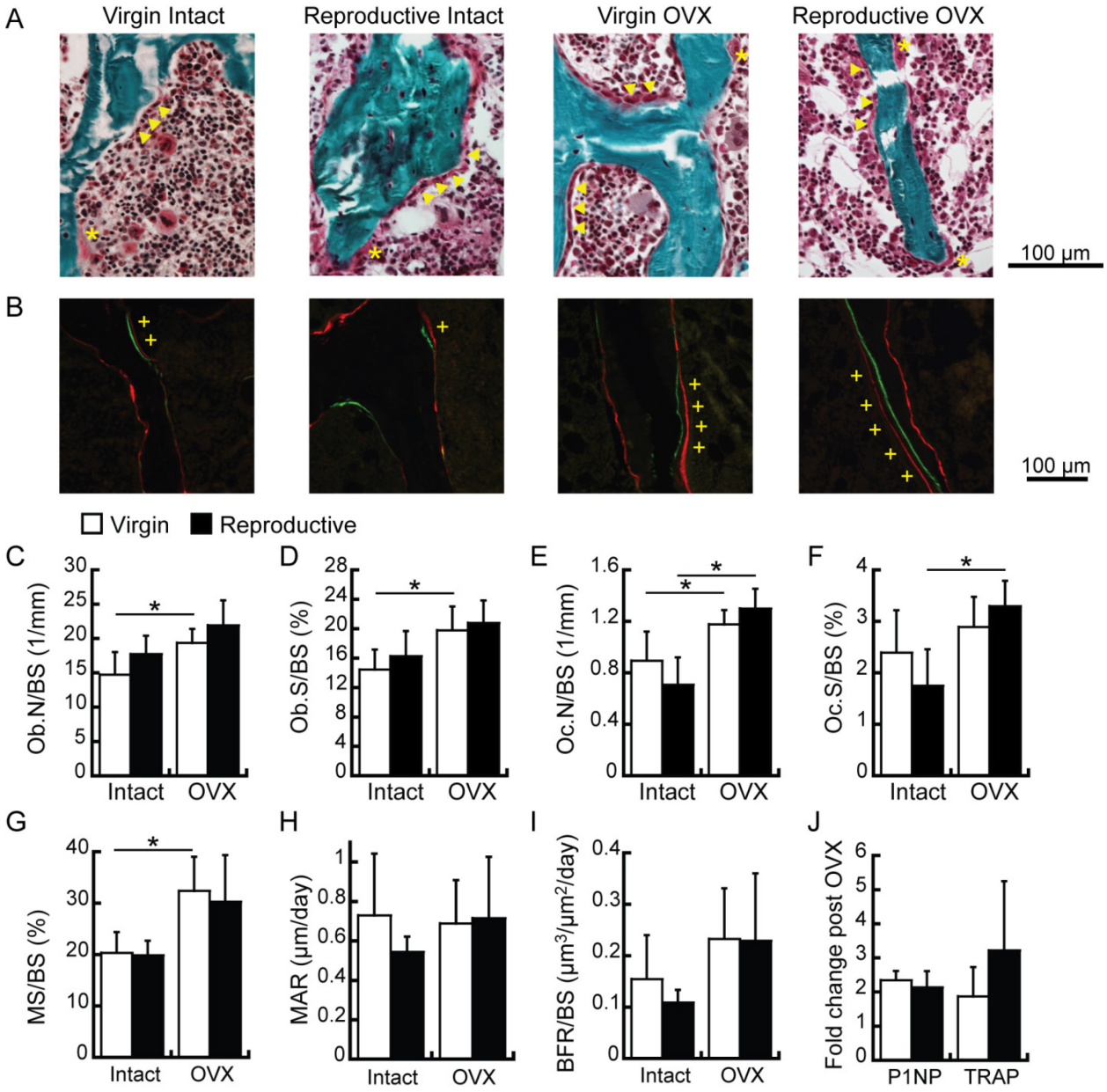

Figure 2. Representative (A) Goldner's trichrome-stained images and (B) fluorochrome labeled images of trabecular bone at the proximal tibia. Osteoblast locations are indicated with yellow triangles; osteoclast locations are indicated with yellow asterisks; fluorochrome double labeled bone surfaces are indicated with yellow plus signs. (C-F) Cell activities, including (C) Ob.N/BS, (D) Ob.S/BS, (E) Oc.N/BS, and (F) Oc.S/BS at 4 weeks post-OVX and in intact rats with and without a reproductive history. (G-I) Bone dynamic histomorphometry parameters, including (G) MS/BS, (H) MAR, and (I) BFR/BS at 8 weeks post-OVX and in intact rats with and without a reproductive history. (J) Fold changes in serum P1NP 2 weeks post OVX and serum TRAP 1 week post OVX in rats with and without a reproductive history. *: significant difference between groups ($p<0.05$).

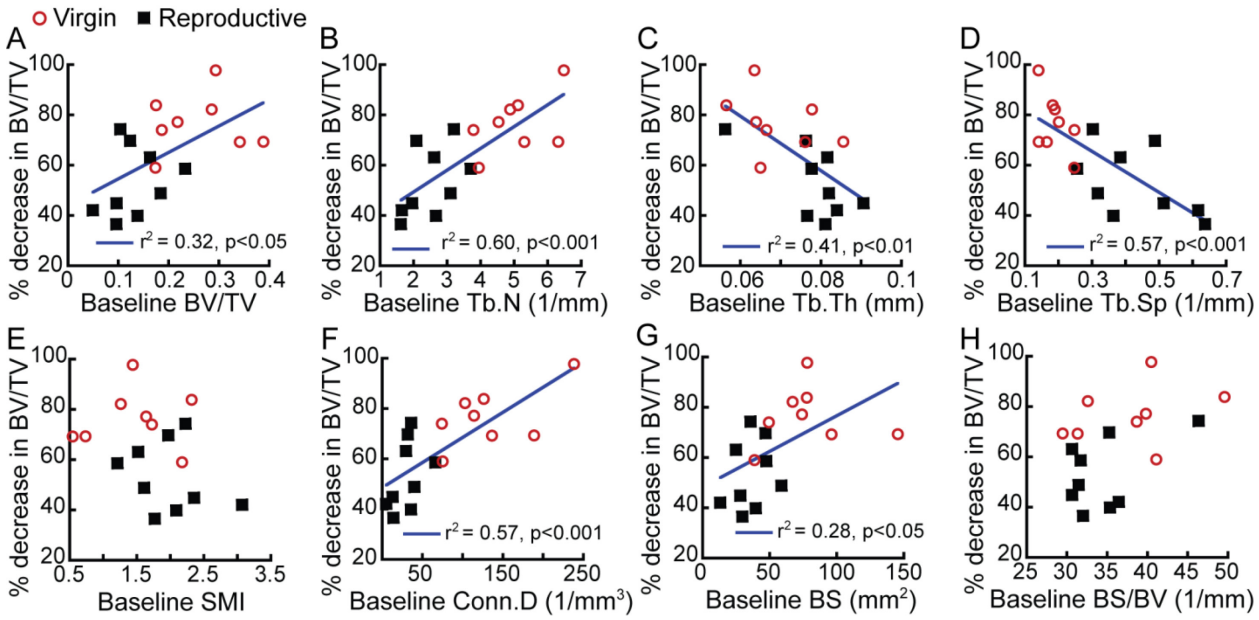

Figure 3. Linear correlations between baseline parameters of trabecular microstructure, including (A) BV/TV, (B) Tb.N, (C) Tb.Th, (D) Tb.Sp, (E) SMI, (F) Conn.D, (G) BS, and (H) BS/BV and the percent decrease in BV/TV over the 12-week post-OVX period.

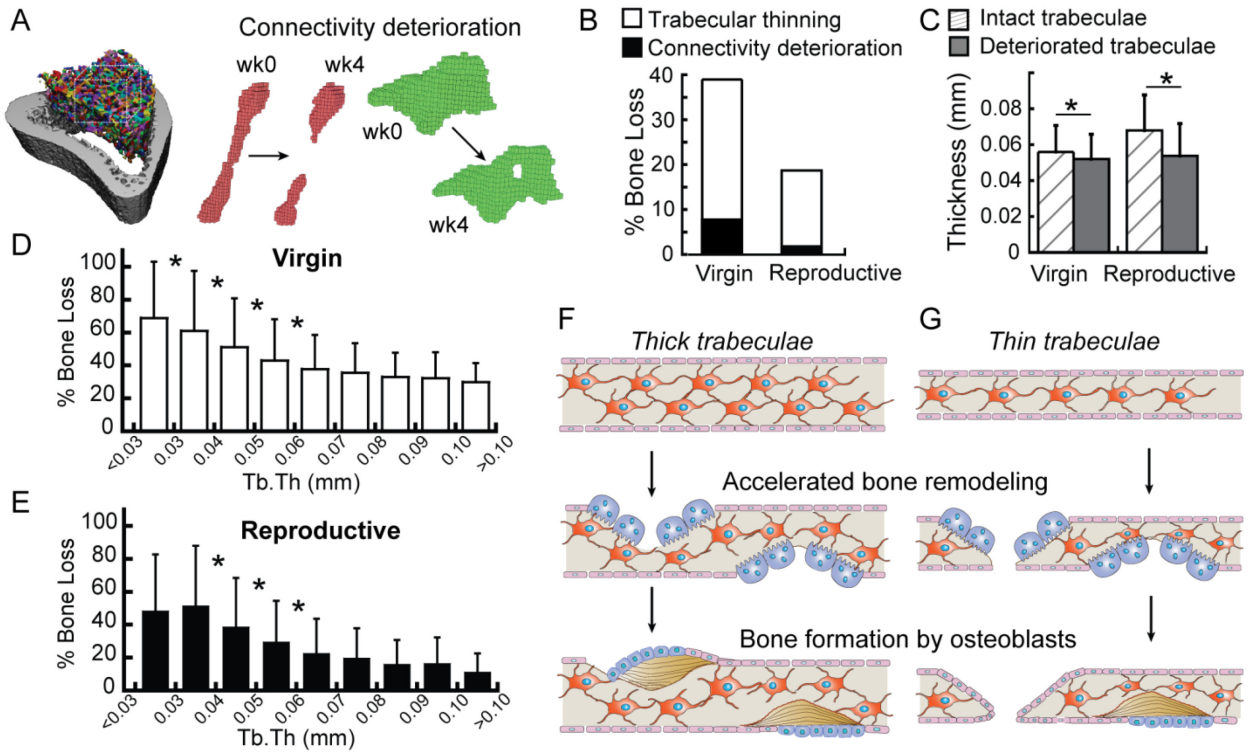

Figure 4. (A) Schematics of ITD analysis. (B) Percent decrease in bone volume due to trabecular thinning and connectivity deterioration over the first 4 weeks post-OVX in virgin and reproductive rats. (C) Mean thickness of trabeculae that remained intact and those undergoing structural deterioration post-OVX. (D-E) Mean percent bone loss of individual trabeculae stratified by thickness in (D) virgin and (E) reproductive rats. (F-G) Schematics of estrogen-deficiency-induced bone resorption, followed by osteoblast-based bone formation in (F) thick and (G) thin trabeculae. *: significant difference between groups ($p<0.05$).

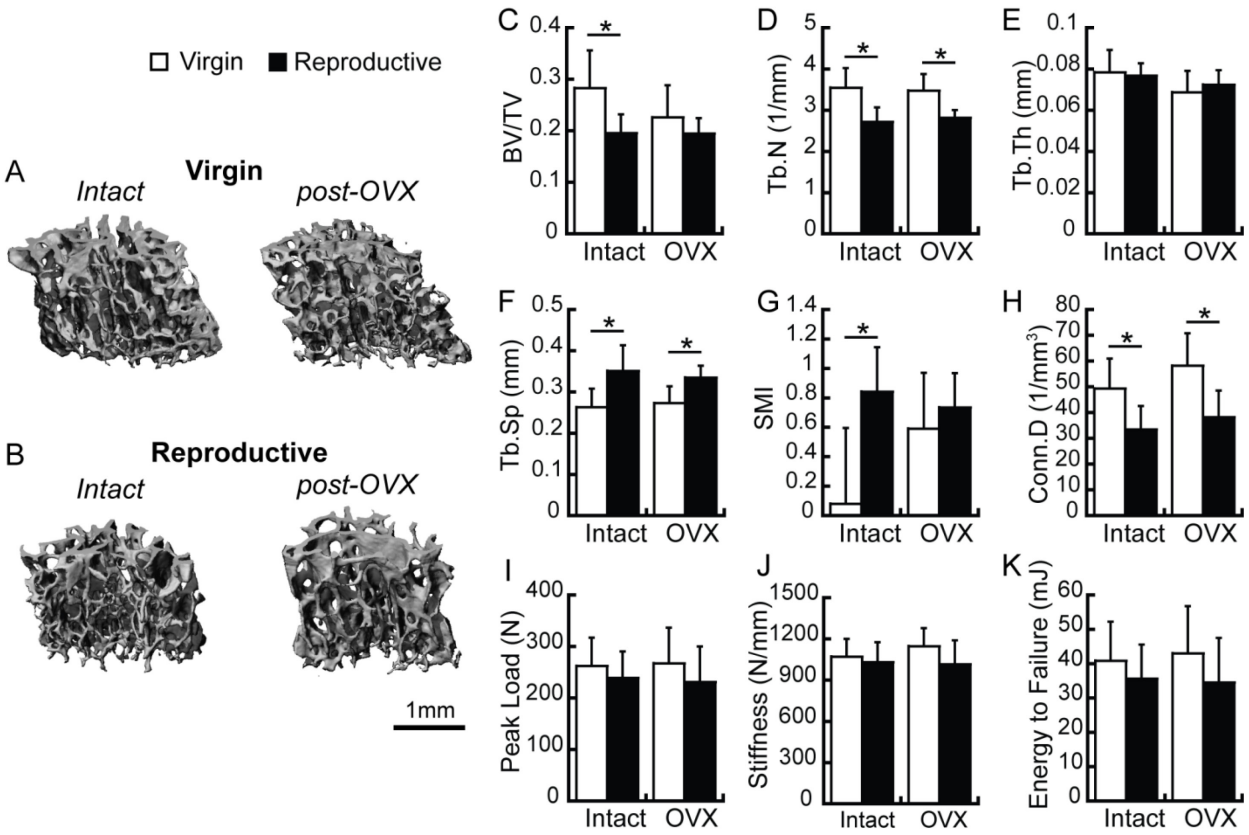

Figure 5. (A-B) Representative 3D renderings illustrating the effects of OVX on trabecular bone at the lumbar vertebra L4 in (A) virgin and (B) reproductive rats. (C-H) Effects of OVX and reproductive history on trabecular microstructure at L4, including (C) BV/TV, (D) Tb.N, (E) Tb.Th, (F) Tb.Sp, (G) SMI, and (H) Conn.D. (I-K) Whole-bone mechanical properties of the lumbar vertebra L2 as a result of OVX and reproductive history, including (I) peak load, (J) stiffness, and (K) energy to failure. * indicate significant differences between groups ($p<0.05$).

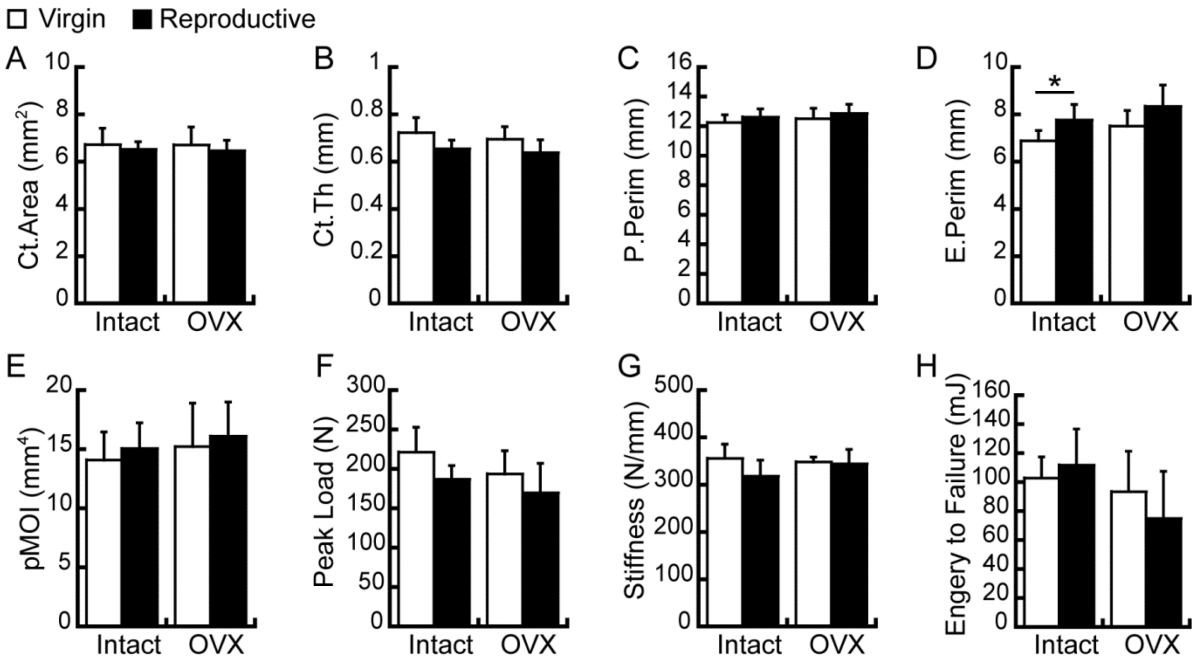

Figure 6. (A-E) Effects of OVX and reproductive history on cortical bone microstructure of the femur midshaft, including (A) Ct.Area, (B) Ct.Th, (C) P.Perim, (D) E.Perim, and (E) pMOI. (F-H) Whole-bone mechanical properties of the femur midshaft as a result of OVX and reproductive history, including (F) peak load, (G) stiffness, and (I) energy to failure. * indicate significant differences between groups ($p<0.05$).

References:

1. Bone Health and Osteoporosis: A Report of the Surgeon General. Rockville, MD: US Department of Health and Human Services, Office of the Surgeon General; 2004.
2. Hui SL, Slemenda CW, Johnston CC, Jr. The contribution of bone loss to postmenopausal osteoporosis. Osteoporos Int. Oct 1990;1(1):30-4. Epub 1990/10/01.
3. Wang Q, Seeman E. Skeletal growth and peak bone strength. Best Pract Res Clin Endocrinol Metab. Oct 2008;22(5):687-700. Epub 2008/11/26.
4. Honda A, Kurabayashi T, Yahata T, Tomita M, Takakuwa K, Tanaka K. Lumbar bone mineral density changes during pregnancy and lactation. Int J Gynaecol Obstet. Dec 1998;63(3):253-8. Epub 1999/02/16.
5. Kalkwarf HJ, Specker BL, Bianchi DC, Ranz J, Ho M. The effect of calcium supplementation on bone density during lactation and after weaning. N Engl J Med. Aug 21 1997;337(8):523-8. Epub 1997/08/21.
6. Karlsson C, Obrant KJ, Karlsson M. Pregnancy and lactation confer reversible bone loss in humans. Osteoporos Int. 2001;12(10):828-34.
7. Sowers M, Corton G, Shapiro B, Jannausch ML, Crutchfield M, Smith ML, et al. Changes in bone density with lactation. Jama. Jun 23-30 1993;269(24):3130-5.
8. Moller UK, Vieth Streym S, Mosekilde L, Rejnmark L. Changes in bone mineral density and body composition during pregnancy and postpartum. A controlled cohort study. Osteoporos Int. Apr 2012;23(4):1213-23. Epub 2011/05/25.
9. Ardeshirpour L, Dann P, Adams DJ, Nelson T, VanHouten J, Horowitz MC, et al. Weaning triggers a decrease in receptor activator of nuclear factor-kappaB ligand expression, widespread osteoclast apoptosis, and rapid recovery of bone mass after lactation in mice. Endocrinology. Aug 2007;148(8):3875-86.
10. Bowman BM, Siska CC, Miller SC. Greatly increased cancellous bone formation with rapid improvements in bone structure in the rat maternal skeleton after lactation. J Bone Miner Res. Nov 2002;17(11):1954-60.
11. Miller SC, Anderson BL, Bowman BM. Weaning initiates a rapid and powerful anabolic phase in the rat maternal skeleton. Biol Reprod. Jul 2005;73(1):156-62. Epub 2005/03/25.
12. Miller SC, Bowman BM. Rapid improvements in cortical bone dynamics and structure after lactation in established breeder rats. Anat Rec A Discov Mol Cell Evol Biol. Feb 2004;276(2):143-9. Epub 2004/01/31.
13. Miller SC, Bowman BM. Rapid inactivation and apoptosis of osteoclasts in the maternal skeleton during the bone remodeling reversal at the end of lactation. Anat Rec (Hoboken). Jan 2007;290(1):65-73. Epub 2007/04/19.
14. Kovacs CS. Maternal Mineral and Bone Metabolism During Pregnancy, Lactation, and Post-Weaning Recovery. Physiol Rev. Apr 2016;96(2):449-547.
15. Brembeck P, Lorentzon M, Ohlsson C, Winkvist A, Augustin H. Changes in cortical volumetric bone mineral density and thickness, and trabecular thickness in lactating women postpartum. The Journal of clinical endocrinology and metabolism. Feb 2015;100(2):535-43. Epub 2014/11/12.
16. Bjornerem A, Ghasem-Zadeh A, Wang X, Bui M, Walker SP, Zebaze R, et al. Irreversible Deterioration of Cortical and Trabecular Microstructure Associated With Breastfeeding. J Bone Miner Res. Oct 13 2016. Epub 2016/10/14.

17. Bornstein S, Brown SA, Le PT, Wang X, DeMambro V, Horowitz MC, et al. FGF-21 and skeletal remodeling during and after lactation in C57BL/6J mice. Endocrinology. Sep 2014;155(9):3516-26. Epub 2014/06/11.
18. Liu XS, Ardeshirpour L, VanHouten JN, Shane E, Wysolmerski JJ. Site-specific changes in bone microarchitecture, mineralization, and stiffness during lactation and after weaning in mice. J Bone Miner Res. Apr 2012;27(4):865-75.
19. de Bakker CM, Altman-Singles AR, Li Y, Tseng WJ, Li C, Liu XS. Adaptations in the Microarchitecture and Load Distribution of Maternal Cortical and Trabecular Bone in Response to Multiple Reproductive Cycles in Rats. J Bone Miner Res. Jan 21 2017. Epub 2017/01/22.
20. Lan S, Luo S, Huh BK, Chandra A, Altman AR, Qin L, et al. 3D image registration is critical to ensure accurate detection of longitudinal changes in trabecular bone density, microstructure, and stiffness measurements in rat tibiae by in vivo micro computed tomography (μCT). Bone. 2013;56(1):83-90.
21. Bouxsein ML, Boyd SK, Christiansen BA, Guldberg RE, Jepsen KJ, Muller R. Guidelines for assessment of bone microstructure in rodents using micro-computed tomography. J Bone Miner Res. Jul 2010;25(7):1468-86.
22. Burghardt AJ, Buie HR, Laib A, Majumdar S, Boyd SK. Reproducibility of direct quantitative measures of cortical bone microarchitecture of the distal radius and tibia by HR-pQCT. Bone. Sep 2010;47(3):519-28.
23. Guo XE, Goldstein SA. Is trabecular bone tissue different from cortical bone tissue? Forma. 1997;12:185-96.
24. Hollister SJ, Brennan JM, Kikuchi N. A homogenization sampling procedure for calculating trabecular bone effective stiffness and tissue level stress. J Biomech. 1994;27(4):433-44.
25. de Bakker CM, Altman AR, Li C, Tribble MB, Lott C, Tseng WJ, et al. Minimizing interpolation bias and precision error in *in vivo* microCT-based measurements of bone structure and dynamics. Annals of biomedical engineering. Jan 19 2016;44(8):2518-28. Epub 2016/01/21.
26. de Bakker CM, Altman AR, Tseng WJ, Tribble MB, Li C, Chandra A, et al. muCT-based, in vivo dynamic bone histomorphometry allows 3D evaluation of the early responses of bone resorption and formation to PTH and alendronate combination therapy. Bone. Apr 2015;73C:198-207. Epub 2015/01/03.
27. Altman AR, De Bakker CM, Tseng WJ, Chandra A, Qin L, Liu XS. Enhanced individual trabecular repair and its mechanical implications in parathyroid hormone and alendronate treated rat tibial bone. Journal of Biomechanical Engineering. 2015;137(1):011004-7. Epub December 10 2014.
28. Pendleton MM, Alwood JS, O'Connell GD, Keaveny TM. Design of Fatigue Test for Ex-Vivo Mouse Vertebra. Proceedings of the 2016 Summer Biomechanics, Bioengineering, and Biotransport Conference. 2016.
29. Liu XS, Sajda P, Saha PK, Wehrli FW, Bevill G, Keaveny TM, et al. Complete volumetric decomposition of individual trabecular plates and rods and its morphological correlations with anisotropic elastic moduli in human trabecular bone. J Bone Miner Res. Feb 2008;23(2):223-35. Epub 2007/10/03.

30. Affinito P, Tommaselli GA, di Carlo C, Guida F, Nappi C. Changes in bone mineral density and calcium metabolism in breastfeeding women: a one year follow-up study. J Clin Endocrinol Metab. Jun 1996;81(6):2314-8. Epub 1996/06/01.
31. Bowman BM, Miller SC. Skeletal mass, chemistry, and growth during and after multiple reproductive cycles in the rat. Bone. Nov 1999;25(5):553-9.
32. More C, Bettembuk P, Bhattoa HP, Balogh A. The effects of pregnancy and lactation on bone mineral density. Osteoporos Int. 2001;12(9):732-7. Epub 2001/10/19.
33. Wiklund PK, Xu L, Wang Q, Mikkola T, Lyytikainen A, Volgyi E, et al. Lactation is associated with greater maternal bone size and bone strength later in life. Osteoporos Int. Jul 2012;23(7):1939-45. Epub 2011/09/20.
34. Waarsing JH, Day JS, Verhaar JA, Ederveen AG, Weinans H. Bone loss dynamics result in trabecular alignment in aging and ovariectomized rats. J Orthop Res. May 2006;24(5):926-35.
35. Altman-Singles AR, Jeong Y, Tseng WJ, de Bakker CM, Zhao H, Lott C, et al. Intermittent Parathyroid Hormone After Prolonged Alendronate Treatment Induces Substantial New Bone Formation and Increases Bone Tissue Heterogeneity in Ovariectomized Rats. J Bone Miner Res. May 03 2017. Epub 2017/05/04.
36. Riis BJ, Hansen MA, Jensen AM, Overgaard K, Christiansen C. Low bone mass and fast rate of bone loss at menopause: equal risk factors for future fracture: a 15-year follow-up study. Bone. Jul 1996;19(1):9-12. Epub 1996/07/01.
37. Jee WS, Yao W. Overview: animal models of osteopenia and osteoporosis. J Musculoskelet Neuronal Interact. Mar 2001;1(3):193-207. Epub 2005/03/11.
38. Martin RB. Porosity and specific surface of bone. Crit Rev Biomed Eng. 1984;10(3):179-222. Epub 1984/01/01.
39. Pivonka P, Buenzli PR, Scheiner S, Hellmich C, Dunstan CR. The influence of bone surface availability in bone remodelling - a mathematical model including coupled geometrical and biomechanical regulations of bone cells. Engineering Structures. 2013;47:134-47.
40. Bjornerem A, Ghasem-Zadeh A, Bui M, Wang X, Rantzau C, Nguyen TV, et al. Remodeling markers are associated with larger intracortical surface area but smaller trabecular surface area: a twin study. Bone. Dec 2011;49(6):1125-30. Epub 2011/08/30.
41. Jepsen KJ, Kozminski A, Bigelow EM, Schlecht SH, Goulet RW, Harlow SD, et al. Femoral Neck External Size but not aBMD Predicts Structural and Mass Changes for Women Transitioning Through Menopause. J Bone Miner Res. Jun 2017;32(6):1218-28. Epub 2017/01/14.
42. Goldman HM, Hampson NA, Guth JJ, Lin D, Jepsen KJ. Intracortical remodeling parameters are associated with measures of bone robustness. Anat Rec (Hoboken). Oct 2014;297(10):1817-28. Epub 2014/06/26.
43. Liu XS, Huang AH, Zhang XH, Sajda P, Ji B, Guo XE. Dynamic simulation of three dimensional architectural and mechanical alterations in human trabecular bone during menopause. Bone. Aug 2008;43(2):292-301.
44. Mosekilde L. Consequences of the remodelling process for vertebral trabecular bone structure: a scanning electron microscopy study (uncoupling of unloaded structures). Bone Miner. 1990;10(1):13-35.

45. Eriksen EF. Normal and pathological remodeling of human trabecular bone: three dimensional reconstruction of the remodeling sequence in normals and in metabolic bone disease. Endocr Rev. Nov 1986;7(4):379-408. Epub 1986/11/01.
46. Li Y, Tseng WJ, De Bakker CM, Zhao H, Liu XS. Relationships between peak bone microstructure and rate of estrogen-deficiency-induced bone loss. Summer Biomechanics, Bioengineering and Biotransport Conference. Tucson, AZ, USA2017. p. #180.
47. de Bakker CMJ, Tseng WJ, Li Y, Zhao H, Altman-Singles AR, Jeong Y, et al. Reproduction Differentially Affects Trabecular Bone Depending on Its Mechanical Versus Metabolic Role. J Biomech Eng. Nov 1 2017;139(11). Epub 2017/10/06.
48. Wronski TJ, Cintron M, Dann LM. Temporal relationship between bone loss and increased bone turnover in ovariectomized rats. Calcif Tissue Int. Sep 1988;43(3):179-83. Epub 1988/09/01.
49. Wronski TJ, Dann LM, Horner SL. Time course of vertebral osteopenia in ovariectomized rats. Bone. 1989;10(4):295-301. Epub 1989/01/01.